Gas phase electronic spectrum of T-shaped AlC_2 radical

C. Apetrei, A. E. W. Knight, E. Chasovskikh, E. B. Jochnowitz, H. Ding, and J. P. Maier

Citation: The Journal of Chemical Physics **131**, 064305 (2009); doi: 10.1063/1.3186758
View online: http://dx.doi.org/10.1063/1.3186758
View Table of Contents: http://aip.scitation.org/toc/jcp/131/6
Published by the American Institute of Physics

Gas phase electronic spectrum of T-shaped AlC_2 radical

C. Apetrei, A. E. W. Knight,[a] E. Chasovskikh, E. B. Jochnowitz, H. Ding,[b] and J. P. Maier[c]
Department of Chemistry, University of Basel, Klingelbergstr. 80, CH-4056 Basel, Switzerland

(Received 28 May 2009; accepted 2 July 2009; published online 12 August 2009)

Gas phase electronic transitions for the $\tilde{C}\ ^2B_2 \leftarrow \tilde{X}\ ^2A_1$ and $\tilde{D}\ ^2B_1 \leftarrow \tilde{X}\ ^2A_1$ band systems of T-shaped AlC_2 (C_{2v}) radical have been measured in the 345–475 nm range. Vibrational analyses of both band systems are reported. Simulation of several rotationally resolved bands confirms previously obtained rotational parameters for the $\tilde{C}\ ^2B_2$ state. The radical is produced by ablating an aluminum rod in the presence of acetylene gas. The resulting supersonic molecular beam is probed using both mass-selective resonant two-color two-photon ionization and laser induced fluorescence. *Ab initio* calculations and vertical electronic excitation energies help the assignment. Vibrational frequencies for the $\tilde{X}\ ^2A_1$, $\tilde{C}\ ^2B_2$, and $\tilde{D}\ ^2B_1$ states have been determined. Rotational analysis of a number of bands yields spectroscopic constants for one vibronic state in the $\tilde{C}\ ^2B_2$ manifold and the origin band of the $\tilde{D}\ ^2B_1 \leftarrow \tilde{X}\ ^2A_1$ system. © *2009 American Institute of Physics*.
[DOI: 10.1063/1.3186758]

I. INTRODUCTION

The relationship between the structure of organometallic species and the nature of the carbon-metal chemical bonding remains a topic of considerable interest. Such clusters provide an opportunity to understand these interactions and to gain insight into the growth mechanisms of metal-carbon nanomaterials. Of these, metal carbides and dicarbides represent an important chemical class with application in a wide range of processes and materials. However, spectroscopic information that could reveal aspects of metal-carbon bonding at the triatomic level is relatively sparse.

Metal-containing carbon compounds are also of interest in astrochemistry, where a few such molecules have been detected in carbon rich astrophysical environments through their microwave and submillimeter/millimeter transitions.[1–3] Because many elements such as magnesium, iron, and sodium are depleted in molecular clouds,[4] the central question concerns the form in which these metal-containing species exist in the interstellar medium (ISM). It is generally believed that the most refractory elements are condensed out onto the surface of dust grains. Unfortunately, knowledge about the gas-phase abundances and the surface absorption of such species in the ISM is limited. Accordingly, the spectroscopic identification of metal-containing molecular carriers has implication for both gas phase and grain chemistry.[3]

To date, 11 main group dicarbides have been investigated spectroscopically (XC_2, X=H, B, C, N, O, Al, Si, P, S, Cl, As).[5] HC_2, NC_2,[6] OC_2,[7] PC_2,[5] SC_2,[8] and AsC_2 (Ref. 5) all possess linear ($C_{\infty v}$) structures. ClC_2 has been shown to have bent shaped $\tilde{X}\ ^2A'$ ground state,[9] while AlC_2 and SiC_2 are T-shaped (C_{2v}).[10,11] Matrix infrared and electronic spectra of BC_2, which is isovalent with AlC_2, have been obtained with features assigned to a cyclic structure.[12,13] As far as heavier systems are concerned, the $\tilde{A}\ ^2A_1 \leftarrow \tilde{X}\ ^2A_1$ transition of the T-shaped YC_2 radical has been studied extensively in vibrational, rotational, and hyperfine detail.[14–16]

At high temperatures, vaporous metal dicarbides are the predominant species in thermodynamic equilibrium with metal-carbon condensed systems.[17–19] Aluminum dicarbide was first detected in a high temperature Knudsen cell using mass spectrometry.[18] The study indicated that the atomization energy of AlC_2 is 1104 ± 21 kJ mol^{-1} and the dissociation energy of Al–C_2 is 514.2 ± 21 kJ mol^{-1}. The latter is slightly higher than the dissociation energy of AlO and thus an apparent exception to the empirical rule that the dissociation energy of a M–C_2 bond is usually 40–130 kJ mol^{-1} less than the corresponding M–O bond.[18]

Photoelectron spectroscopy of AlC_2^- revealed a vibrational progression of 590 cm^{-1}, which was assigned as the stretching mode of the neutral Al–C_2.[20] Theoretical calculations provided estimates for all three vibrational frequencies for AlC_2; none of these have been observed in the infrared.[10,21,22]

Ablation of an aluminum rod in the presence of a C_2H_2/He gas mixture together with photoionization mass spectrometry with 7.9 eV photons yielded ions at m/z 51 consistent with the mass of AlC_2. The implication that AlC_2 possesses a stable structure in the gas phase was established using laser induced fluorescence (LIF). Confirmation of its T-shaped (C_{2v}) structure emerged from the measurement of the $\tilde{C}\ ^2B_2 \leftarrow \tilde{X}\ ^2A_1$ transition of AlC_2. Rotational analysis for the origin band provided estimates for the $\tilde{C}\ ^2B_2$ state molecular parameters.[10]

In this paper the gas-phase electronic spectrum of AlC_2 is investigated over a broad spectral range using both a mass-

[a]On sabbatical leave from Molecular Dynamics Laboratory, School of Science, Griffith University, Brisbane, Australia.
[b]Present address: School of Physics and Optoelectronic Technology, Dalian University of Technology, Dalian, People's Republic of China.
[c]Author to whom correspondence should be addressed. Electronic mail: j.p.maier@unibas.ch.

selective resonant two-color two-photon ionization (R2C2PI) technique and LIF. The $\tilde{C}\ ^2B_2 \leftarrow \tilde{X}\ ^2A_1$ origin band has been confirmed and new vibronic bands are observed. *Ab initio* calculations on T-shaped AlC_2 (C_{2v}) have been carried out to guide the assignments.

II. EXPERIMENTAL

Jet cooled AlC_2 was produced using laser vaporization of an aluminum rod (30 mJ/5 ns pulse from a 532 nm Nd:Yttrium aluminium garnet focused to 0.3 mm) in the presence of a 1%–5% acetylene gas mixture seeded in either helium or argon provided by a 0.3 mm orifice pulsed valve. The rod was rotated and translated so that a fresh surface was continuously exposed to the laser, which was fired to coincide with the gas flow over the target area. The ablation plume flows through a channel (3 mm diameter, 5–15 mm long) before entering vacuum. The resulting free-jet expansion is probed using the mass-selective R2C2PI technique[23] or LIF.

R2C2PI spectra were collected by probing the skimmed beam of the jet expansion. Ions were removed by applying a perpendicular electric field before entering the ionization region of a Wiley–McLaren time-of-flight mass spectrometer.[24] Neutral molecules were irradiated with a pulse of tunable ultraviolet-visible (UV-Vis) radiation, followed by 7.9 eV photons from an F_2 excimer laser. Ions were then extracted into a time-of-flight tube where the signal from a microchannel plate ion detector was sent to a fast oscilloscope and data acquisition card. The combination of the UV-Vis and the 157 nm photons was sufficient to ionize AlC_2. Low resolution spectra for the vibronic survey scans were collected over the 345–500 nm range using an OPO system ($\sim 5\ cm^{-1}$ bandwidth). A pulsed dye laser was used ($\sim 0.15\ cm^{-1}$ bandwidth, ~ 5 mJ/pulse) for the rotationally resolved work, with calibration through the use of an optogalvanic spectrum obtained from a Fe/Ne hollow cathode lamp.

LIF spectra were measured using an excimer pumped dye laser (bandwidth of $0.15\ cm^{-1}$). Fluorescence signal was collected by an $f/1$ lens and detected using a photomultiplier and digital oscilloscope.

III. THEORETICAL CALCULATIONS

The electronic ground state structures of AlC_2 were investigated using both coupled cluster RCCSD(T) theory[25] and the hybrid density B3LYP functional[26] with Dunning's correlation-consistent basis sets.[27] The calculations indicate that T-shaped AlC_2 (C_{2v}) is a global minimum. Linear AlCC ($C_{\infty v}$) and CAlC ($D_{\infty h}$) are local minima lying approximately 0.4 and 7 eV higher in energy, respectively.

Equilibrium geometries for the ground state were optimized using the B3LYP/aug-cc-pVQZ theory and RCCSD(T)/cc-pVTZ approach. Previously[10] theoretical calculations of excited electronic states of AlC_2 (C_{2v}) were carried out using the complete active space self-consistent field method (CASSCF) (Ref. 28) and multireference configuration interaction (MRCI) theory.[29] Vertical excitation energies were calculated for states up to 3.8 eV above the ground state. In order to predict the spectrum in the UV region, higher lying states for AlC_2 (C_{2v}) have been investigated with CASSCF and MRCI approaches using the GAUSSIAN 98 suite of programs[30] and MOLPRO package.[31] The resulting vertical transition energies and oscillator strengths are summarized in Table I.

TABLE I. Calculated vertical transition energies (T_v) and oscillator strengths (f) with CASSCF, MRCI, and MRCI+Q theories with cc-pVTZ basis sets for T-shaped AlC_2 (C_{2v}).

	T_v (eV)			f
Transition	CAS	MRCI	MRCI+Q	CAS
$\tilde{A}\ ^2A_1 \leftarrow \tilde{X}\ ^2A_1$	1.19	1.27	1.49	2.8×10^{-2}
$\tilde{B}\ ^2B_1 \leftarrow \tilde{X}\ ^2A_1$	2.21	2.37	2.46	7.5×10^{-4}
$\tilde{C}\ ^2B_2 \leftarrow \tilde{X}\ ^2A_1$	2.76	2.83	2.73	1.5×10^{-2}
$\tilde{D}\ ^2B_1 \leftarrow \tilde{X}\ ^2A_1$	2.97	3.31	3.31	7.8×10^{-3}
$\tilde{E}\ ^2B_2 \leftarrow \tilde{X}\ ^2A_1$	3.59	3.89	3.83	1.5×10^{-2}
$\tilde{F}\ ^2A_1 \leftarrow \tilde{X}\ ^2A_1$	4.21			1.8×10^{-3}
$\tilde{G}\ ^2A_2 \leftarrow \tilde{X}\ ^2A_1$	4.70			0.0

IV. RESULTS AND DISCUSSIONS

The R2C2PI low resolution ($\sim 5\ cm^{-1}$ bandwidth) electronic spectra of the $\tilde{C}\ ^2B_2 \leftarrow \tilde{X}\ ^2A_1$ and $\tilde{D}\ ^2B_1 \leftarrow \tilde{X}\ ^2A_1$ systems of AlC_2 for the 345–475 nm range are shown in Figs. 1 and 2, respectively. The wavelengths of the vibronic bands (maxima) and suggested assignments are listed in Table II.

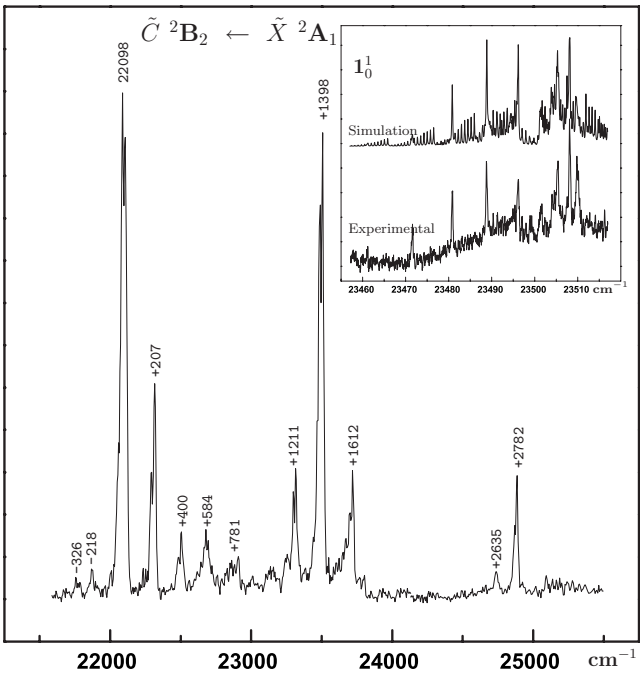

FIG. 1. Low resolution ($5\ cm^{-1}$ bandwidth) spectrum of the $\tilde{C}\ ^2B_2 \leftarrow \tilde{X}\ ^2A_1$ electronic system and high resolution ($0.15\ cm^{-1}$ bandwidth) spectrum of the $+1398\ cm^{-1}$ band (inset) for the T-shaped AlC_2 radical, recorded in the range of 21 000–26 000 cm^{-1} using a resonant two-color two-photon ionization technique in a supersonic molecular beam.

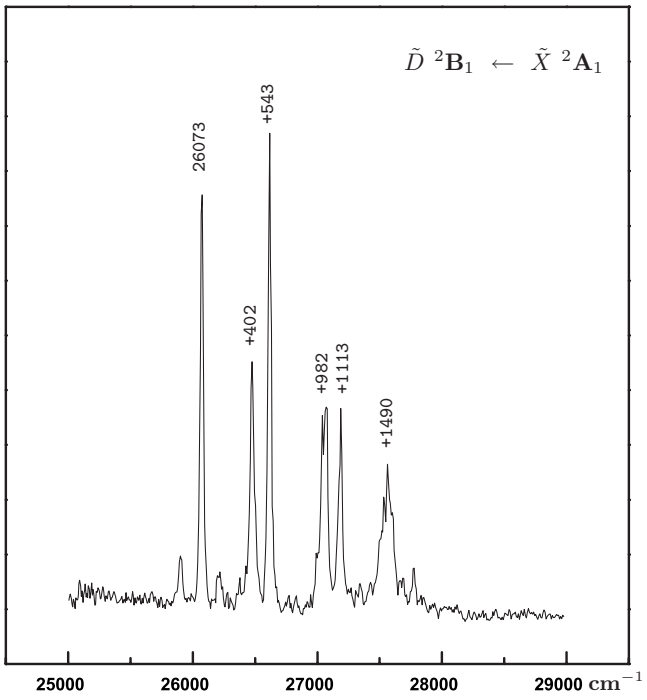

FIG. 2. Low resolution resonant two-color two-photon ionization spectrum of the $\tilde{D}\ ^2B_1 \leftarrow \tilde{X}\ ^2A_1$ electronic system for the T-shaped AlC_2 radical, recorded in the range 24 000–29 000 cm^{-1} in a supersonic molecular beam.

A. $\tilde{C}\ ^2B_2 \leftarrow \tilde{X}\ ^2A_1$

Previous coupled cluster calculations [CCSD(T)] estimate the harmonic frequencies of ground state $\tilde{X}\ ^2A_1$ AlC_2 as ν_1=1735 (a_1), ν_2=645 (a_1), and ν_3=421 (b_2) cm^{-1}.[10] These frequencies were thus used as a starting point in assigning the low resolution $\tilde{C}\ ^2B_2 \leftarrow \tilde{X}\ ^2A_1$ spectrum depicted in Fig. 1. Higher resolution rotationally resolved spectra were obtained to assist in confirming the most probable identities of the vibrational bands.

TABLE II. Vibrational band maxima (cm^{-1}) in the $\tilde{C}\ ^2B_2 \leftarrow \tilde{X}\ ^2A_1$ and $\tilde{D}\ ^2B_1 \leftarrow \tilde{X}\ ^2A_1$ band systems of AlC_2.

		Assignment
$\tilde{\nu}$	$\Delta\tilde{\nu}$	$\tilde{C}\ ^2B_2 \leftarrow \tilde{X}\ ^2A_1$
22 098	0.0	0_0^0
22 305	207	2_0^1
22 498	400	2_0^2
22 682[a] (22 678, 22 713)	584 (580, 613)	3_0^1, 2_0^3
22 879	781	$3_0^1 2_0^1$
23 309	1211	3_0^2
23 496	1398	1_0^1
23 710	1612	$2_0^1 1_0^1$
24 733	2635	$3_0^2 1_0^1$
24 880	2782	1_0^2
		$\tilde{D}\ ^2B_1 \leftarrow \tilde{X}\ ^2A_1$
26 073	0.0	0_0^0
26 475	402	3_0^2
26 616	543	2_0^1
27 055	982	$3_0^2 2_0^1$
27 186	1113	2_0^2
27 563	1490	1_0^1, 2_0^3, $3_0^2 2_0^2$

[a]Higher resolution studies show that the band at 22 682 cm^{-1} actually consists of two overlapping bands at 22 678 and 22 713 cm^{-1}.

TABLE III. Molecular parameters (cm^{-1}) determined from the least squares fit of the spectrum for AlC_2, $\tilde{C}\ ^2B_2 \leftarrow \tilde{X}\ ^2A_1$ (1_0^1) and $\tilde{D}\ ^2B_1 \leftarrow \tilde{X}\ ^2A_1$ (0_0^0). Values in parenthesis denote 2σ standard deviation. Optimized geometries for the $\tilde{X}\ ^2A_1$, $\tilde{C}\ ^2B_2$ (0_0^0), and $\tilde{D}\ ^2B_1$ (0_0^0) state at CASSCF and SA-CASSCF level of theories.

	$\tilde{X}\ ^2A_1$[a]	$\tilde{C}\ ^2B_2$	$\tilde{D}\ ^2B_1$
		1_0^1	0_0^0
A	1.7093(107)	1.5695(98)	1.743(50)
B	0.4052(50)	0.4035(50)	0.355(49)
C	0.3228(49)	0.321(45)	0.295(94)
T_0		23499.7(2)	26083.2(2)
r_{Al-C} (Å)	1.276[a]	1.950[a]	2.095[b]
r_{C-C} (Å)	1.928[a]	1.321[a]	1.27[b]
α_{C-Al-C} (deg)	38.7[a]	39.6[a]	35.3[b]

[a]Reference 10.
[b]Reference 33.

The observed rotational structure of the $\tilde{C}\ ^2B_2 \leftarrow \tilde{X}\ ^2A_1$ origin band of AlC_2 is consistent with that expected for an electric dipole allowed perpendicular b-type transition in a C_{2v} molecule.[10] Accordingly, transitions involving a_1 modes are also electric dipole allowed and will be observed as b-type perpendicular. However, those involving nontotally symmetric b_2 vibrations in the absence of vibronic coupling are only allowed as even quantum changes (i.e., Franck–Condon allowed). These $\Delta v = \pm 2$ transitions will also display rotational contours with b-type perpendicular band structure. Using these guidelines, assignments may be made, starting with the dominant 22 108 cm^{-1} band in Fig. 1, which has been already confirmed as the origin.[10]

The partially rotational resolved R2C2PI spectrum of the +1398 cm^{-1} band in the $\tilde{C}\ ^2B_2 \leftarrow \tilde{X}\ ^2A_1$ transition is shown in the inset of Fig. 1, accompanied by a spectral simulation, assuming a b-type perpendicular band for a near-prolate symmetric top, performed using the WANG program.[32] The band is assigned as the 1_0^1 transition, where ν_1 is the C=C stretching mode. The measured excited state ($\tilde{C}$) frequency of ν_1'=1398 cm^{-1} compares with the calculated ground state frequency for ν_1'' of 1735 cm^{-1}. The reduction in the C=C stretching frequency relative to the ground state is consistent with the lengthening of the C=C bond in the $\tilde{C}$ state (both calculation and estimated rotational constants are in support of this). The significant Franck–Condon activity in ν_1 is also consistent with the appreciable lengthening of the C=C bond in the $\tilde{C}$ state relative to the ground state. Spectroscopic constants for ν_1' vibronic level have been estimated from the spectral simulation with constants reported in Table III. However it must be recognized that difficulties can arise in fitting the finer features of the observed spectrum due to the potential perturbations in the $\tilde{C}\ ^2B_2$ manifold arising as a result of interactions with rovibronic levels of the underlying $\tilde{B}$ state.[10] Nevertheless the simulation is quite acceptable.

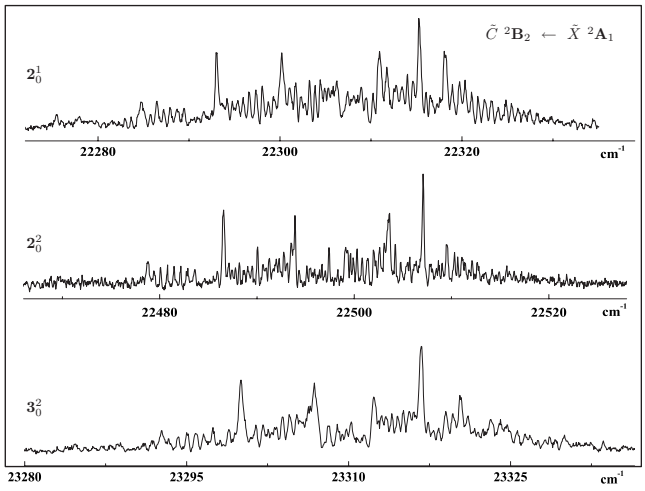

FIG. 3. Rotationally resolved LIF spectra (0.15 cm^{-1} bandwidth) of the 22 305, 22 498, and 23 309 cm^{-1} transitions in the $\tilde{C}\ ^2B_2 \leftarrow \tilde{X}\ ^2A_1$ AlC_2 band system.

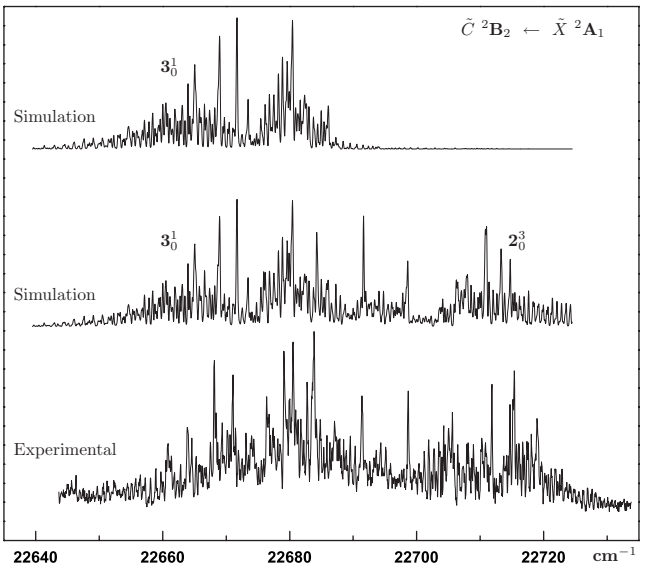

FIG. 4. Rotationally resolved LIF spectrum (0.15 cm^{-1} bandwidth) of the $\tilde{C}\ ^2B_2 \leftarrow \tilde{X}\ ^2A_1$ AlC_2 band system (Fig. 1, +584 cm^{-1}). Rotational contour simulations for an *a*-type parallel and a mixture of both *a*-type parallel band and *b*-type perpendicular bands are shown above the experimental spectrum.

The second progression member in ν_1', i.e., the 1_0^2 transition, is observed at +2782 cm^{-1} (Fig. 1) and displays a *b*-type perpendicular rotational band contour with shape quite similar to those shown in Fig. 3, thus being associated with transition involving progressions in a_1 modes or even-quantum-change overtones.

Figure 3 displays the LIF detection (0.15 cm^{-1} resolution) of three vibronic bands observed at +207, +400, and +1211 cm^{-1} with respect to the origin. The extended *K*-rotational structure observed for all three bands is consistent with its interpretation as a *b*-type perpendicular bands for a near-prolate symmetric top. The intensity of the +207 cm^{-1} band is approximately one-third that of the origin, while that for +400 cm^{-1} is less again by a factor of approximately 4. The pattern of relative intensities, as well as the contour being the same as that of the origin band, is consistent with a progression in a totally symmetric mode. Accordingly, the +207 and +400 cm^{-1} bands are assigned as first two progression members involving the ν_2 (Al–C_2 stretch), with an approximate value of $\nu_2'=207$ cm^{-1}. The appreciable anharmonicity observed is consistent with a large frequency change occurring for ν_2 between the $\tilde{X}$ and $\tilde{C}$ states (the calculated value for ν_2'' is 645 cm^{-1}), indicating a much shallower ν_2 potential function in the $\tilde{C}$ state. The 2_0^2 transition, middle plot, overlaps with the 0-0 and 1-1 bands of the $\tilde{B}\ ^4\Sigma^- \leftarrow \tilde{X}\ ^4\Sigma^-$ AlC transition, therefore the trace shown has been obtained using a normalized spectral substraction to remove the contamination from the AlC diatomic fluorescence. This was possible due to the fact that the above mentioned transition in AlC has a longer fluorescence lifetime than that of AlC_2, thus allowing the collection of a decongested spectrum of the diatomic through gating the tail end of the LIF decay and later subtracting it from the total signal containing fluorescence from both species.

The band observed at +1211 cm^{-1} from the origin (Fig. 1) shown in high resolution detail as the bottom trace in Fig. 3 is due to the Franck–Condon allowed $\Delta v=2$ transition involving excitation in ν_3, i.e., 3_0^2. This yields an approximate frequency of 605 cm^{-1} for ν_3 in the $\tilde{C}$ state.

Based on the assignment $\nu_2'=207$ cm^{-1} for the $\tilde{C}$ state, the two bands observed toward lower energy from the $\tilde{C}\ ^2B_2 \leftarrow \tilde{X}\ ^2A_1$ origin (Fig. 1, −218 and −326 cm^{-1}) are both candidates for the 2_1^1 sequence band. Our preferred assignment for the −326 cm^{-1} band is 2_1^1, which yields $\nu_2''=533$ cm^{-1} compared to $\nu_2''=645$ cm^{-1} from calculation. Despite the supersonic free jet environment, vibrational cooling may not be that efficient in the helium carrier gas, hence it is not unexpected that there is thermal population in the ν_2'', $v=1$ level.

The band observed at +1612 cm^{-1} was also partially rotationally resolved using LIF detection and exhibits a *b*-type perpendicular *K*-structure. The frequency is close to the combination of the observed frequencies for ν_1' and ν_2', i.e., 1398+207=1605 cm^{-1}. Accordingly, this transition is assigned as the $2_0^1 1_0^1$ combination band.

Finally, the LIF spectrum (0.15 cm^{-1} resolution) recorded in the region near 440 nm (Fig. 1, +584 cm^{-1}) is presented in Fig. 4. Measurement at higher resolution provides clear indication that this does not conform to a *b*-type perpendicular transition. Figure 4 includes rotational band contour simulations for an *a*-type parallel band centered at ~22 678 cm^{-1} and a *b*-type perpendicular band (intensity ~30% that of the parallel band) at ~22 713 cm^{-1}. The third member of the ν_2 progression, i.e., 2_0^3 excitation, is expected to lie in this region and would be responsible for the *b*-type perpendicular band. Added together, this combined simulation matches the overall spectral structure in the region 22 640–22 740 cm^{-1} quite well.

An *a*-type parallel band derives intensity from the dipole-allowed T_z transition moment, implying that the vibronic symmetry associated with the +584 cm^{-1} band is A_1. The conclusion advanced is that the +584 cm^{-1} band corre-

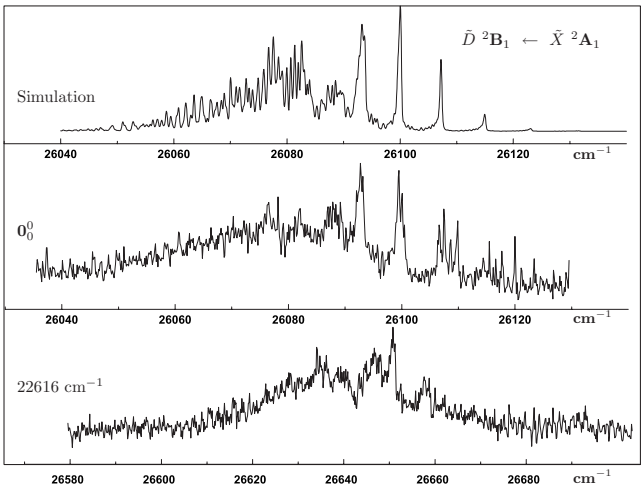

FIG. 5. Rotationally resolved resonant two-color two-photon ionization spectra (0.15 cm^{-1} bandwidth) of the two strongest bands observed in the $\tilde{D}\ ^2B_1 \leftarrow \tilde{X}\ ^2A_1$ system. A rotational contour simulation for a *c*-type $^2B_1 \leftarrow {}^2A_1$ transition is shown in the top trace.

sponds to the transition 3_0^1, where the ν_3 vibrational mode (b_2 symmetry; $\tilde{C}$ state vibronic symmetry$=b_2 \otimes B_2 = A_1$) derives intensity through vibronic coupling with the strong, T_z dipole-allowed $\tilde{A}\ ^2A_1 \leftarrow \tilde{X}\ ^2A_1$ transition. The $\tilde{A}$ state is calculated to lie approximately 12 000 cm^{-1} below the $\tilde{C}$ state. The fact that the ν_3, $v=1$ vibrational frequency increased in the $\tilde{C}$ state relative to the $\tilde{X}$ state (ν_3 ground state frequency calculated as 421 cm^{-1}) is consistent with the $\tilde{A}\ ^2A_1$ electronic state, from which intensity is borrowed, lying lower in energy than the $\tilde{C}$ state. Hence we conclude that the +584 cm^{-1} band is composed of a stronger constituent due the vibronically allowed 3_0^1 transition together with a lesser contribution from the Franck–Condon allowed 2_0^3 progression member (Table II).

The attribution of the +781 cm^{-1} band in Fig. 1 as $3_0^1 2_0^1$ follows from the observed displacement of ~+200 cm^{-1} relative to the 3_0^1 vibronically induced progression origin. Assignment of the +1211 cm^{-1} band as 3_0^2 is based on the anticipated Franck–Condon intensity for this transition.

Finally, we consider the band at −218 cm^{-1} (toward lower energy) from the $\tilde{C}\ ^2B_2 \leftarrow \tilde{X}\ ^2A_1$ origin. A candidate for its assignment might be the 3_1^1 sequence band. However, based on the estimate, $\nu_3' = 580$ cm^{-1} from the measured position of the 3_0^1 transition, this assignment would imply that $\nu_3'' = 580 + 218 = 798$ cm^{-1}. This appears to be too high given the values for ν_3'' derived from theory (~400–450 cm^{-1}).[10] An alternative assignment is the hot band $3_1^0 2_0^1$, which would yield $\nu_3'' = 207 + 218 = 425$ cm^{-1}.

B. $\tilde{D}\ ^2B_1 \leftarrow \tilde{X}\ ^2A_1$

The two strongest UV bands found in the $\tilde{D}\ ^2B_1 \leftarrow \tilde{X}\ ^2A_1$ band system (Fig. 2, bands at 26 073 and +543 cm^{-1}) were investigated further at higher resolution (0.15 cm^{-1}) with R2C2PI and are shown in Fig. 5. The bands could also be recorded using LIF but due to other overlapping features in this UV region the spectra are congested and more complicated to analyze.

The rotational band profiles are matched successfully with a simulation assuming a conventional Hamiltonian for an asymmetric top considering a *c*-type perpendicular transition in a C_{2v} molecule (dipole allowed T_x transition moment). The simulation compares favorably with the experimental trace for the 26 073 cm^{-1} band. Despite poorer signal to noise for the 26 616 cm^{-1} band, the simulation is acceptable. Attempts to match the measured rotational profile for the 26 073 cm^{-1} band with either a *b*-type perpendicular or *a*-type parallel simulation proved unsuccessful. Accordingly, these are assigned as belonging to another electronic band system, presumably the T_x electric dipole allowed $\tilde{D}\ ^2B_1 \leftarrow \tilde{X}\ ^2A_1$ transition. Recent calculations (SA-CASSCF geometry optimization, Table III),[33] estimate that the $\tilde{D}\ ^2B_1$ state energy is in vicinity of 3.1 eV (~25 000 cm^{-1}), lending further support to the assignment of the AlC_2 vibronic structure in the 24 000–28 000 cm^{-1} region as being due to the $\tilde{D}\ ^2B_1 \leftarrow \tilde{X}\ ^2A_1$ transition. Assignments for the vibrational structure observed are discussed below and presented in Table II.

The dominant progression forming mode in the $\tilde{D}\ ^2B_1 \leftarrow \tilde{X}\ ^2A_1$ transition appears to be ν_2, in contrast with the activity observed in ν_1 for the $\tilde{C} \leftarrow \tilde{X}$ excitation. The ν_2 vibrational mode is principally the Al–C_2 symmetric stretch. As may be deduced from the inertial parameters emerging from the *c*-type band contour simulation shown in Fig. 5, the Al–C bond length, hence the Al–C_2 perpendicular distance, changes appreciably in the $\tilde{D}$ state relative to the ground state ($\tilde{D}$:1.996 Å; $\tilde{X}$:1.819 Å; $\Delta = 0.165$ Å), and considerably more than between the $\tilde{C}$ and $\tilde{X}$ states ($\Delta = 0.016$ Å).[10] This large geometric change along the ν_2 normal coordinate associated with $\tilde{D} \leftarrow \tilde{X}$ excitation confirms the assignment of ν_2 as the dominant progression forming mode in the $\tilde{D}\ ^2B_1 \leftarrow \tilde{X}\ ^2A_1$ transition. The displacements for the transitions 2_0^1 and 2_0^2 are +543 and 1113 cm^{-1}, respectively. It is clear that the interval (570 cm^{-1}) between ν_2', $v=1$ and $v=2$ suggests a significant positive anharmonicity.

Figure 2 shows a relatively strong transition at +402 cm^{-1} displacement from the origin. The assignment offered is the Franck–Condon allowed $\Delta v = 2$ transition in ν_3, i.e., 3_0^2. No band is observed at twice this displacement from the $\tilde{D}\ ^2B_1 \leftarrow \tilde{X}\ ^2A_1$ origin, hence the +402 cm^{-1} band cannot be the first member of a progression in an a_1 mode (the only possibility would be ν_1, but in any case the observed frequency is far too low for ν_1 to be a valid candidate). The observed transition cannot be 3_0^1 because the vibronic symmetry for the 3^1 level, assuming that this is the $\tilde{D}\ ^2B_1 \leftarrow \tilde{X}\ ^2A_1$ transition, is $b_2 \otimes B_1 = A_2$ and the A_2-A_1 transition moment is zero for a C_{2v} molecule.

Assignments follow for the bands at +982 and 1113 cm^{-1} as $3_0^2 2_0^1$ and 2_0^2. However, it is necessary to address two questions regarding this, as well as the relatively large anharmonicity in the ν_2 progression. First, the 3_0^2 assigned band is quite strong for a ν_3', $v=2$ Franck–Condon

TABLE IV. Experimentally determined vibrational frequencies (cm^{-1}) for the two electronic systems.

	$\tilde{X}\,^2A_1$		$\tilde{C}\,^2B_2$	$\tilde{D}\,^2B_1$
	ω	$\tilde{\nu}$	$\tilde{\nu}$	$\tilde{\nu}$
ν_1	1735[a]	⋯	1398(5)[b]	1490(5)[b]
ν_2	645[a]	533(5)[c]	207(5)[b]	543(5)[b]
ν_3	421[a]	425(5)[c]	580(5)[b]	201(5)[d]

[a]Calculated, Ref. 10.
[b]This work.
[c]This work (based on the assigned hot bands).
[d]By dividing double quanta excitations.

allowed transition. Second, the positions for $3_0^2 2_0^1$ and 2_0^2 appear a little abnormal. The most likely cause of these anomalies is a Fermi resonance between ν_3', $v=2$, and ν_2', $v=1$. This would be a classic case of $3^2\cdots 2^1$ coupling via cubic anharmonicity (the well known ground state stretch-bend coupling in CO_2 being the pedagogical example).[34] This explanation is supported by the appearance of the structure in the +982, 1113 cm^{-1} region, which is relatively broad and indicative of the expected Fermi triad arising from the coupling between $3^4\cdots 3^2 2^1\cdots 2^2$. Likewise, the broad structure in the +1490 cm^{-1} region would be due to the corresponding Fermi quartet. Modeling of these possible Fermi resonances is outside the scope of this paper. It is likely that the first progression member of the ν_1 mode, i.e., 1_0^1, may also lie among this structure.

C. Vibronic coupling

The estimates for the AlC_2 vibrational frequencies derived for both the $\tilde{C}$ and $\tilde{D}$ states are summarized in Table IV. In the $\tilde{C}$ state, ν_2 is reduced considerably from its ground state value ($\nu_2'=207$ cm^{-1} versus $\nu_2''=533$ cm^{-1}). The 2^1 level is of B_2 vibronic symmetry. The drop in frequency is consistent with the proposal that the $\tilde{E}$ ($^2B_2$) state, calculated ~7500 cm^{-1} above the $\tilde{C}$ state, perturbs levels of B_2 symmetry in the $\tilde{C}$ state.

Vibronic coupling between states in two interacting manifolds does involve all vibrational levels of appropriate symmetry. However, the dominant interactions are between like states with $\Delta v=\pm 1$ differences in vibrational quantum numbers.[35,36] Hence, the $v=0$ level of the $\tilde{C}$ state will interact with the ν_2, $v=1$ level in the higher $\tilde{E}$ ($^2B_2$) state. In contrast, the ν_2, $v=1$ level of the $\tilde{C}$ state will be coupled with both the ν_2, $v=0$ and $v=2$, levels of the $\tilde{E}$ ($^2B_2$) state.

From simple perturbation theory $|\text{energy shift}| = |H_{ij}^2/(E_j-E_i)|$, where H_{ij}^2 is the vibronic coupling interaction matrix element and $\Delta E=E_j-E_i$ is the energy difference between the coupled states. Furthermore, the coupling matrix elements (for harmonic oscillator wave functions) are related by the relationship $\langle v+1|H_{ij}|v\rangle=\sqrt{v}\langle 1|H_{ij}|0\rangle$. Accordingly, a simple coupling scheme is used to obtain estimates for the shifts in vibrational energy levels due to vibronic coupling. The coupling matrix elements in the range ~1000–3000 cm^{-1} are typical for coupling between electronically excited states.[35,36]

A modest vibronic coupling matrix element of ~1050 cm^{-1} (with $\Delta E=7500$ cm^{-1} taken as energy gap between the $\tilde{C}$ and $\tilde{E}$ states) is sufficient to "push down" the ν_2, $v=1$ level in the $\tilde{C}$ state by ~300 cm^{-1} relative to what might be an unperturbed frequency for ν_2' of ~500 cm^{-1} (based on $\nu_2''=533$ cm^{-1}). This could explain the considerably reduced frequency for ν_2 observed for the $\tilde{C}$ state.

The estimates for ν_3'' and ν_3' are 425 and 580 cm^{-1}. The question arises as to why ν_3 is *increased* in the $\tilde{C}$ state relative to the $\tilde{X}$ state. Observe that ν_3 is of symmetry species b_2, hence the vibronic symmetry of the 3^1 level is $b_2\otimes B_2=A_1$. As established above from rotational contour simulations, the 3_0^1 transition arises as a result of vibronic coupling. The A_1 electronic state (with significant oscillator strength) that is most likely to be responsible for the intensity borrowing is the *lower* lying $\tilde{A}\,^2A_1$ state, calculated as lying ~12 000 cm^{-1} below the $\tilde{C}$ state. From calculations analogous to those discussed above for ν_2, a coupling matrix element of ~900 cm^{-1} is sufficient to "push up" the 3^1 level by ~160 cm^{-1} in the $\tilde{C}$ state relative to its (calculated) frequency of ~420 cm^{-1} in the $\tilde{X}$.

Analogous arguments may be applied to rationalize the frequencies for ν_2 and ν_3 observed in the $\tilde{D}$ state. The 2^1 level is observed at +543 cm^{-1}. This in fact is little different from it's ground state frequency of 533 cm^{-1}. The vibronic symmetry of 2^1 in the $\tilde{D}$ state is B_1. Moreover, the nearest B_1 electronic state with which the $\tilde{D}$ state can couple is the *lower* $\tilde{B}\,^2B_1$ state, ~6700 cm^{-1} below. Thus one would anticipate that, if anything, ν_2 might increase in frequency in the $\tilde{D}$ state. The observed frequency of 543 cm^{-1} is consistent with the proposal that it has been pushed up, relative to its unperturbed frequency, as a result of vibronic coupling with the *lower* lying $\tilde{B}\,^2B_1$ state.

The ν_3 vibronic frequency in the $\tilde{D}$ state, derived from the observation of the 3_0^2 band at +402 cm^{-1} is approximately 200 cm^{-1}. This contrasts with ν_3 in the $\tilde{X}$ state, derived from the spectrum of ~425 cm^{-1}. The vibronic symmetry of 3^1 in the $\tilde{D}(^2B_1)$ state is A_2. The only A_2 state nearby in AlC_2 is $\tilde{G}(^2A_2)$ state, calculated ~12 500 cm^{-1} *above* the $\tilde{D}$ state. A vibronic coupling matrix element of ~1150–1200 cm^{-1} would be sufficient to depress the 3^1 level in the $\tilde{D}$ state by the requisite amount of ~220–250 cm^{-1}. While the above arguments are indicative rather than quantitative, they serve to rationalize the observed frequencies for ν_2 and ν_3 observed in the $\tilde{C}$ and $\tilde{D}$ electronic states of AlC_2.

V. CONCLUSION

Vibrational structure in the electric dipole allowed $\tilde{C}\,^2B_2\leftarrow\tilde{X}\,^2A_1$ and $\tilde{D}\,^2B_1\leftarrow\tilde{X}\,^2A_1$ transitions has been mea-

sured with both LIF and mass selective R2C2PI spectroscopy. Rotational contour measurements have been carried out at higher resolution for a selection of the stronger bands in both systems. Assignments are provided for the Franck–Condon activity involving ν_1 and ν_2 in the $\tilde{C}\,^2B_2 \leftarrow \tilde{X}\,^2A_1$ transition, as well as vibronic activity in ν_3 due to coupling with the strong dipole allowed $\tilde{A}\,^2A_1 \leftarrow \tilde{X}\,^2A_1$ excitation. The strong Franck–Condon activity in the ν_1 mode (C=C stretch) is consistent with the observed $\tilde{C}\,^2B_2 \leftarrow \tilde{X}\,^2A_1$ geometry change, deduced from rotational band contour simulations, which involved appreciable lengthening of the C=C bond. In the higher lying $\tilde{D}\,^2B_1 \leftarrow \tilde{X}\,^2A_1$ transition, the Franck–Condon activity is dominated by an intense progression involving ν_2 (Al–C_2 stretch). This assignment is supported by an appreciable change in the Al–C bond length and hence Al–C_2 perpendicular distance, estimated from rotational band contour simulation assuming an *c*-type perpendicular transition. The simulations confirm the attribution of the excitation as $\tilde{D}\,^2B_1 \leftarrow \tilde{X}\,^2A_1$. No vibronic activity in ν_3 is possible for this transition because of symmetry constraints. However, there is evidence of $3^2 \ldots 2^1$ coupling via cubic anharmonicity in the $\tilde{D}$ vibrational manifold. New estimates for vibrational frequencies and rotational parameters are thereby provided for the $\tilde{C}$ and $\tilde{D}$ states of AlC_2 (Table IV).

ACKNOWLEDGMENTS

This work is supported by the Swiss National Science Foundation (Project No. 200020-124349/1). A.K. thanks the Maier group for their friendship and hospitality during his stay in Basel.

[1] M. Guelin, J. Cernicharo, C. Kahane, and J. Gomez-Gonzalez, Astron. Astrophys. **157**, 17 (1986).
[2] K. Kawaguchi, E. Kagi, T. Hirano, S. Takano, and S. Saito, Astrophys. J. Lett. **406**, L39 (1993).
[3] M. A. Anderson and L. M. Ziurys, Astrophys. J. Lett. **452**, L157 (1995).
[4] U. J. Sofia, J. A. Cardelli, and B. D. Savage, Astrophys. J. **430**, 650 (1994).
[5] F. X. Sunahori, J. Wei, and D. J. Clouthier, J. Am. Chem. Soc. **129**, 9600 (2007).
[6] N. Oliphant, A. Lee, P. F. Bernath, and C. R. Brazier, J. Chem. Phys. **92**, 2244 (1990).
[7] H. Abe, M. Mukai, M. Fujitake, and N. Ohashi, J. Mol. Spectrosc. **195**, 317 (1999).
[8] A. J. Schoeffler, H. Kohguchi, K. Hoshina, Y. Ohshima, and Y. Endo, J. Chem. Phys. **114**, 6142 (2001).
[9] Y. Sumiyoshi, T. Ueno, and Y. Endo, J. Chem. Phys. **119**, 1426 (2003).
[10] E. Chasovskikh, E. B. Jochnowitz, E. Kim, I. Navizet, and J. P. Maier, J. Phys. Chem. A **111**, 11986 (2007).
[11] D. L. Michalopoulos, M. E. Geusic, P. R. R. Langridgesmith, and R. E. Smalley, J. Chem. Phys. **80**, 3556 (1984).
[12] J. M. L. Martin, P. R. Taylor, J. T. Yustein, T. R. Burkholder, and L. Andrews, J. Chem. Phys. **99**, 12 (1993).
[13] M. Wyss, M. Grutter, and J. P. Maier, J. Phys. Chem. A **102**, 9106 (1998).
[14] T. C. Steimle, A. J. Marr, J. Xin, A. J. Merer, K. Athanassenas, and D. Gillet, J. Chem. Phys. **106**, 2060 (1997).
[15] R. R. Bousquet and T. C. Steimle, J. Chem. Phys. **114**, 1306 (2001).
[16] T. C. Steimle, R. R. Bousquet, K. C. Namiki, and A. J. Merer, J. Mol. Spectrosc. **215**, 10 (2002).
[17] F. J. Kohl and C. A. Stearns, J. Chem. Phys. **52**, 6310 (1970).
[18] C. A. Stearns and F. J. Kohl, J. Phys. Chem. **77**, 136 (1973).
[19] E. E. Filby and L. L. Ames, Inorg. Nucl. Chem. Lett. **8**, 855 (1972).
[20] A. I. Boldyrev, J. Simons, X. Li, and L. S. Wang, J. Am. Chem. Soc. **121**, 10193 (1999).
[21] G. V. Chertihin, L. Andrews, and P. R. Taylor, J. Am. Chem. Soc. **116**, 3513 (1994).
[22] X. G. Zheng, Z. H. Wang, and A. C. Tang, J. Phys. Chem. A **103**, 9275 (1999).
[23] H. Ding, T. W. Schmidt, T. Pino, A. E. Boguslavskiy, F. Guthe, and J. P. Maier, J. Chem. Phys. **119**, 814 (2003).
[24] W. C. Wiley and I. H. McLaren, Rev. Sci. Instrum. **26**, 1150 (1955).
[25] J. D. Watts, J. Gauss, and R. J. Bartlett, J. Chem. Phys. **98**, 8718 (1993).
[26] A. D. Becke, J. Chem. Phys. **98**, 5648 (1993).
[27] D. E. Woon and T. H. Dunning, J. Chem. Phys. **98**, 1358 (1993).
[28] H. J. Werner and P. J. Knowles, J. Chem. Phys. **82**, 5053 (1985).
[29] H. J. Werner and P. J. Knowles, J. Chem. Phys. **89**, 5803 (1988).
[30] M. J. Frisch, G. W. Trucks, H. B. Schlegel *et al.*, GAUSSIAN98, Revision A.7, Gaussian Inc., Pittsburgh, PA, 1998.
[31] MOLPRO, a package of ab initio programs designed by H.-J. Werner and P. J. Knowles, version 2006.1.
[32] D. Luckhaus and M. Quack, Mol. Phys. **68**, 745 (1989).
[33] R. Linguerri, private communication, 2007.
[34] G. Herzberg, *Molecular Spectra and Molecular Structure* (van Nostrand, New York, 1945).
[35] G. Fischer, *Vibronic Coupling: The Interaction Between the Electronic and Nuclear Motions* (Academic, New York, 1984).
[36] W. D. Lawrance and A. E. W. Knight, J. Phys. Chem. **94**, 1249 (1990).